Accepted Manuscript

Synthesis and properties of a graphene-like macrocycle based on tetraphenylethene

Han Wang , Tingting Lin , Ji Ma , Weizhi Wang

PII: S0040-4020(14)00864-3

DOI: 10.1016/j.tet.2014.06.018

Reference: TET 25683

To appear in: *Tetrahedron*

Received Date: 10 March 2014

Revised Date: 4 May 2014

Accepted Date: 3 June 2014

Please cite this article as: Wang H, Lin T, Ma J, Wang W, Synthesis and properties of a graphene-like macrocycle based on tetraphenylethene, *Tetrahedron* (2014), doi: 10.1016/j.tet.2014.06.018.

Graphical Abstract

Leave this area blank for abstract info.

Synthesis and properties of a graphene-like macrocycle based on tetraphenylethene

Han Wang, Tingting Lin, Ji Ma, Weizhi Wang*

Tetrahedron
journal homepage: www.elsevier.com

Synthesis and properties of a graphene-like macrocycle based on tetraphenylethene

Han Wang,[a] Tingting Lin,[b] Ji Ma,[a] Weizhi Wang*[a]

[a] State Key Laboratory of Molecular Engineering of Polymers, Department of Macromolecular Science, Fudan University, Shanghai 200433, China.
[b] Institute of Materials Research and Engineering, A*STAR (Agency for Science, Technology and Research), 3 Research Link, Singapore 117602

ARTICLE INFO

Article history:
Received
Received in revised form
Accepted
Available online

Keywords:
tetraphenylethene
macrocycle
McMurry coupling
mobilities
graphene

ABSTRACT

In this work, tetraphenylethene macrocycles are selectively synthesized in one step from McMurry coupling reaction of 1,1-bis(4-phenylcarbonyl)-2,2-diphenylethene in 45% overall yield. A more planar cyclized compound can be obtained by oxidization of tetraphenylethene macrocycles with iron (III) chloride in nitromethane. Their unusual optical properties and electrical properties are explored. The measured mobilities are 0.7022 and 0.0055 $cm^2 V^{-1} s^{-1}$, respectively. The decomposition temperatures are also measured by thermal gravimetric analysis as respectively 342 °C and 455 °C, indicating good thermal stabilities. The understanding of the structure and properties will benefit to the chemical synthesis of graphene.

1. Introduction

Since the breakthrough in graphene discovery[1], the applications for desirable properties of graphene have never failed to lose attractions to scientists. Based on high performances,[2-6] graphene and its derivatives are promising materials for electronic and optical devices, such as organic field-effect transistors (FETs),[7,8] transparent electrodes,[9] and solar cells[10] etc.

Preparation of graphene is generally divided into top-down and bottom-up methods. Top-down method, which is quick and simple, is limited in some extents. Mechanical exfoliation of highly oriented pyrolytic graphite (HOPG) can provide a small amount of pure graphene,[1] while it cannot meet the requirement for large scale production. Chemical exfoliation of expanded graphite oxide can produce graphene sheets in larger quantity,[11] but it is inevitable to introduce heteroatoms such as oxygen, which are detrimental to the performances of graphene. The other method, bottom-up synthesis of graphene is efficient, such as epitaxial growth on SiC or chemical vapor deposition (CVD), .[12-14] Since the requirement of well-defined structures and supermolecular assembles of graphene materials began to rise,[15,16] syntheses of graphene structures by small organic molecules become noticeable for its atomic accuracy. Müllen K. and colleagues developed an efficient method to synthesize polycyclic aromatic hydrocarbons by Diels – Alder additions or alkyne trimerizations and further cyclodehydrogenations.[17-20] The largest graphene molecule acquired previously possesses 222 carbons and a diameter of 3 nm.[21] Fasel's group synthesized graphene nanoribbon (GNRs) by surface-assisted coupling to yield GNRs of different topologies with atomic accuracy by controlling the monomers.[22] To our knowledge, the research on graphene macrocycles is rarely reported. The synthesis of cyclacenes is inspiring for the research of carbon nanotubes.[23,24] Explorations in synthesizing graphene macrocycles could also provide more information on graphene. Herein, we introduce McMurry coupling of carbonyl containing tetraphenylethene (TPE) monomers to produce a TPE-based macrocycle (TM, shown in Scheme 1) selectively at a yield of 45%. Then, the TM molecule was dehydrogenized by $FeCl_3/CH_3NO_2$ to give a more planar TMC molecule. MALDI-TOF was used to monitor the reaction procedure and detect the final product.[25] As TPE is a typical aggregation-induced emission (AIE) luminogens,[26] TM should also possess significant AIE properties. In our further experiments, TM performed different optical properties in its solution. The photoluminescence peak of TM shift bathochromically with an increasing of concentration. Optical and electrical tests of TM and TMC and density functional theory (DFT) calculations were carried out to help examine their properties. High thermal stabilities of TM and TMC were also characterized by TGA. It is worthy investigating the structures and properties of the yielded conjugated macrocycles to provide knowledge to chemical syntheses of graphene.

2. Results and discussion

2.1 Syntheses of monomers, TM and TMC

* Corresponding author. Tel.: +86 21-65640293.
E-mail address: weizhiwang@ustc.edu (W.Z. Wang)

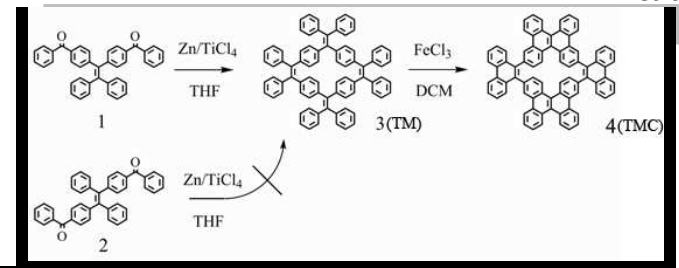

Scheme 1. The synthesis of TM and TMC.

The synthesis of two monomers by Friedel – Crafts reaction is based on our former research.[27] It can be inferred that the Friedel – Crafts benzoylation of tetraphenylethene possess distinct configurational isomers. After separation, two isomers, which are discriminated by the positions of benzoyl groups, were obtained. The NMR spectra and single crystal diffractions have determined the structures of the two isomers: 1,1-bis(4-phenylcarbonyl)-2,2-diphenylethene (monomer **1**) and 1,2-bis(4-phenylcarbonyl)-1,2-diphenylethene (monomer **2**) (see Table. S1, ESI†).

Scheme 1 describes the McMurry self-coupling of monomers. In a typical preparation, monomer **1** was added to a previous prepared $Zn/TiCl_4$/THF solution and the reaction was kept at 66 ℃ for 24 h. The reaction solution was inspected by MALDI-TOF and it showed two peaks at 510 and 1016 (as shown in Fig. 1). The peak at 1016 belongs to TM. The peak at 510 is a reduction by-product of monomer **1**. After purification, the total yield of TM was 45%. Using the same coupling process and characterization for monomer **2**, no TM peak at 1016 was detected. The identified peaks were attributed to non-cycled products of two molecules coupling (as shown in Fig. S1). From these results, a possible reaction mechanism can be derived. First, a monomer comes to the surface of zero-valent titanium [Ti (0)], which has been formed by the reduction of $TiCl_4$/Zn. Second, two monomers are induced to cross-couple and form a pinacol dimer by the Ti (0). Finally, the carbonyl-coupling reaction gives a pinacol deoxygenation to yield the desired alkene.

The results are closely related to the monomer structural characteristics and the reaction mechanism. The structure of monomer **1** allows four oxygen atoms of the pinacolate dimer to approach and bond on a common Ti (0) surface. This step is important to the formation of the cycled structure. In contrast, monomer **2** cannot react in this way to give TM. As only one oxygen atom from each monomer can attach to the same catalyst surface, the final products are opened structure dimers. The solvent used in the reaction has two effects on the yield of TM. First, it can affect the conformation of Ti (0), such as the particle size, surface area, and physical nature of the surface (edges, corners, holes). The second is the relative solubility of the monomer and product in a given solvent. For a solvent to increase the yield of TM, the monomer should be very soluble in it, but TM should be insoluble. This prevents the coupling reaction at the dimer stage. The McMurry coupling of the two monomers was incipiently designed to synthesize different polymerized chain consisted of TPE blocks. However, there is a very small peak of trimer but no peak of higher molecular weight in MALDI-TOF mass spectra. This is in accordance with the former explanation that the later coupling is prohibited by both the steric hindrance of phenyl rings and low solubility of the dimer.

The nearly planar TMC can then be prepared by the oxidation of TM (50 mmol) by $FeCl_3$ (20 mmol) in DCM (100 mL) at room temperature in 40 min. This method has been used previously in the synthesis of polycyclic aromatic hydrocarbons.[19] The oxidation is a step-by-step dehydrogenation, and TM can give oxidized product TMC by losing 6 pairs of hydrogen atoms. The MALDI-TOF and ^{1}H-NMR spectra of TM and TMC are shown in Fig. S2-4. The more planar molecule ($C_{80}H_{40}$, Table S3) cannot be obtained by $FeCl_3$ because of its low oxidizing ability and the twisted structure of TMC. When $AlCl_3$ was used instead of $FeCl_3$, the more planar molecule ($C_{80}H_{40}$) can be seen in the MALDI-TOF spectra (not given). However, as the oxidization proceeds, there was a series of peaks with intervals of 16 (exactly the molar mass of an oxygen atom) in MALDI-TOF spectra, indicating that the products were readily to react with oxygen to yield impurity. The additional by-products meant the purification became more difficult, even after careful removal of oxygen. The major oxidation product TMC was separated from its by-products by column chromatography. Results of MALDI-TOF-MS and ^{1}H NMR suggested TMC molecule was the product losing 12 hydrogen atoms from TM. While there might exist isomers in the final product, the confirmation of the structure of TMC was based on both experimental results and DFT calculations. The energy band gaps measured by optical (Fig. 3) and cyclic voltammetry tests (Table S2) coincided with band gaps of TMC molecule by DFT calculations (Table S3) than other isomers, which pointed out that TMC was the most reasonable structure.

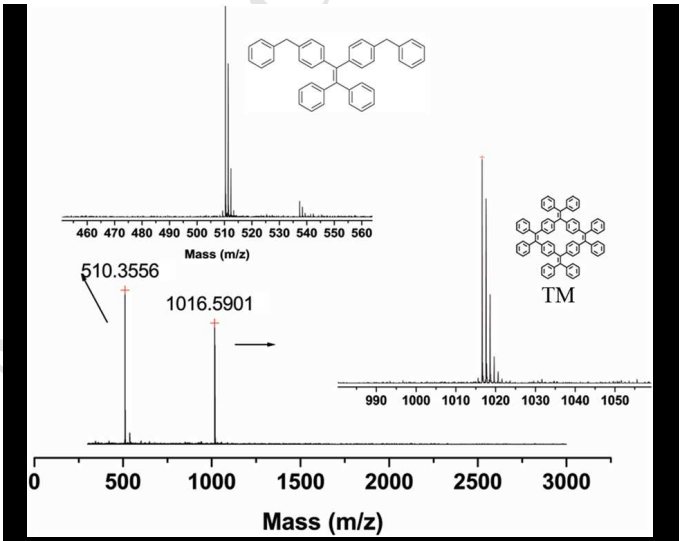

Fig. 1 MALDI-TOF mass spectra of McMurry coupling product TM and its byproduct for monomer **1**.

2.2. Optical properties

Even being same in composition, the optical properties of the two monomers are different. The two monomers possess different fluorescence in their solid states and solutions. Monomer **1** is white under natural light and emits blue fluorescence under UV irradiation. In comparison, monomer **2** is yellow under natural light and emits green fluorescence under UV irradiation (Fig. 2a). The bathochromic shifts in absorption and fluorescence spectra in solid state and solutions (Fig. 2b) are possibly due to their different configurations and conformations.

TM performed unusual optical properties observed in our former syntheses. The solid powder of TM purified from the recrystallization procedure emitted blue fluorescence, while when treated with a few solvent, the fluorescence turned evidently to yellow-green. This phenomenon drew our attention to further investigation on its optical properties.

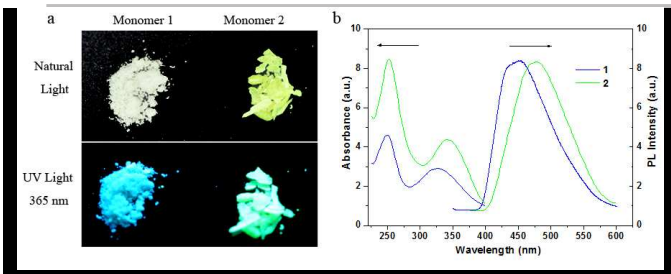

Fig. 2 (a) The appearance of monomer **1** and **2** in natural light and UV irradiation. (b) The absorption and photoluminescence (PL) spectra of monomer **1** and **2** solutions. The absorption peaks of monomer **1** are 250 nm, 342 nm and of monomer **2** are 252 nm, 342 nm, respectively. The PL peak of monomer **2** is 15 nm red-shifted (at 476 nm) to monomer **1** (at 451 nm).

TM is a white powder under natural light. When irradiated at 365 nm, it has a bright blue emission (Fig. 3a) at 446 nm. The UV absorption curve has a broad, shapeless peak at 365 nm with a small shoulder at 275 nm. This indicates that TM adopts varied conformations in the solid state. On the other hand, TM is composed of four AIE active TPE units and should also exhibit the AIE effect. The emission intensity of pure TM in DCM solution (3.0 μM) increases fourfold after adding 20 wt% of petroleum ether (shown in Fig. S5). This elevation in PL intensity was attributed to the aggregation-induced enhanced emission (AIEE) effect of TM in the petroleum ether. THF is a relatively good solvent for TM, while TM is insoluble in petroleum ether. Adding proportion poor solvent (petroleum ether) to the THF solution of TM induces TM molecules to aggregate. This aggregation leads to the restrictions of phenyl rings intramolecular rotations and thus decreases the non-radiative deactivation process, which finally enhance the emission intensity.[28] Furthermore, we found the TM emission dependent on the concentration. When the concentration of TM in DCM increasing from 0.1 to 3 μM (Fig. 3c), the emission changes from 453 nm (blue) to 530 nm (yellow green). At high concentrations, TM forms aggregates that are very crowded and have little free volume. This induces the TM molecule to adopt a less twisted conformation. These structures tend to be more conjugated, especially for the inner TM molecules of the aggregates, and cause a red shift in the emission. In diluted solutions, on the other hand, TM has a deep blue emission due to the larger free volumes and a more twisted structure. However, in the solid state where the structure should be the most rigorously confined, the emission comes at 446 nm. This is smaller than in both the diluted solution and as an aggregate.

To determine the cause of this unusual result, we first examined the emissive properties of TMC. The emission of TMC is also dependent on the concentration. Fig. 3d shows the emission of TMC in DCM with increasing concentration (inset, from left to right). The emission peak moves from 510 nm to 539 nm as the concentration increases from 0.2 to 10 μM. Furthermore, the intensity also increases with the increasing concentration. The TMC molecule, with its less twisted structure, should readily form aggregates by π-π interaction. As the concentration increases, the molecules are more likely to aggregate, which lowers the energy band-gap and leads to the red-shift of emission peak. This interaction becomes even stronger in a solid film. Compared with the solution sample, the emission of a solid TMC film consequently peaks at 600 nm (Fig. 3b). This is a large red shift of 61 nm.

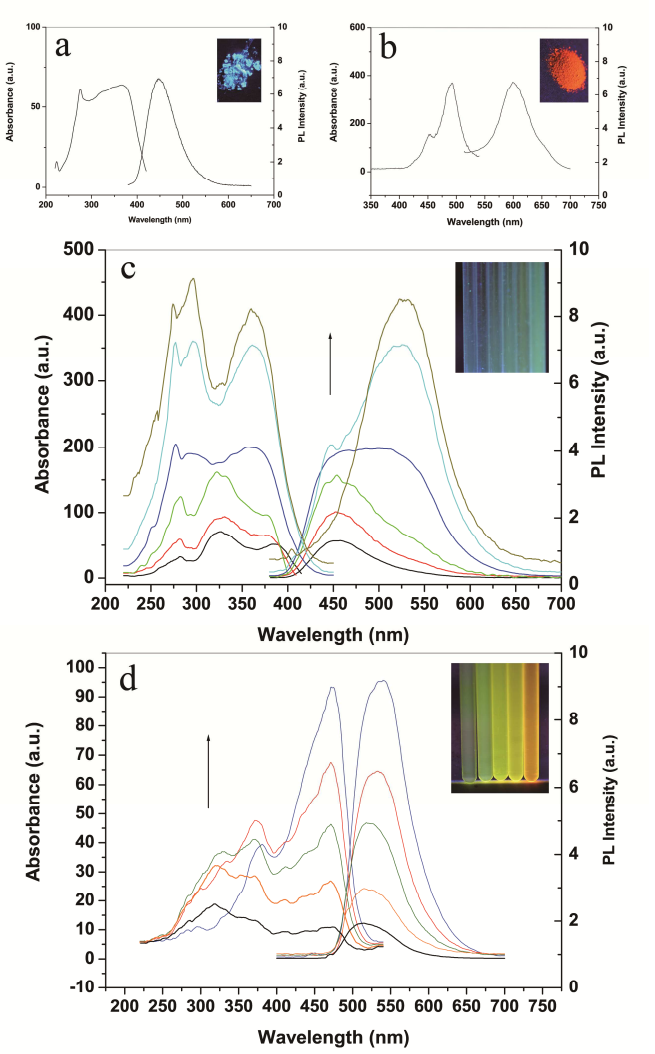

Fig. 3 The optical properties of TM and TMC at room temperature. (a) A solid film of TM, (b) A solid film of TMC, (c) TM in DCM, from 0.1 to 3 μM, (d) TMC in DCM, from 0.2 to 10 μM. For samples c and d, the concentration increases from left to right, irradiated at 365 nm.

These results show how the morphology and structure of molecule have a dramatic effect on its emission properties. Blue, green, yellow and red emissions can be obtained. To understand the relationship between structure and emission, we used molecular calculations. TM acts like a big cyclohexane molecule and adopts different conformers such as “boat”, “chair” or planar depending on the environment. In a solid film, the TM molecule adopts the most twisted structure and the shortest conjugated unit. The calculated occupied volume of each molecule is 969.57 $Å^3$, and surface area is 978.32 $Å^2$. The compact structure easily forms crystals as proved by the XRD data of TM (Fig. 4). Once dissolved, TM adopts a more extended structure. The calculated solvent volume and area increase to 2690.12 $Å^3$ and 1279.42 $Å^2$, respectively. TMC is the oxidized product of TM and has the less twisted conformation, which gives it a longer conjugation and improves the formation of aggregates. It also has smaller calculated occupied volume (893.12 $Å^3$), and surface area (842.86 $Å^2$). The decrease in area and volume continues for the more planar molecule ($C_{80}H_{40}$, Table S3) although we were not successful in obtaining experimental data for this molecule. This suggests that this molecule would have the largest red shift in the emission.

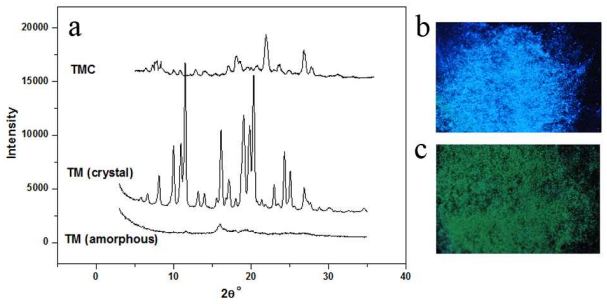

Fig. 4 (a) XRD results of crystal, amorphous TM and TMC powder. Crystal (b) and amorphous (c) TM powder under 365 nm irradiation. The amorphous TM powder was obtained after physical grinding by pestle and mortar.

Fig. 4 shows the powder X-ray diffraction experiments of TM and TMC. The highest peak for TM comes at 2θ = 12°, which gives a distance of 0.34 nm. The less twisted molecule, TMC, has the highest peak at 2θ = 22° and a distance of 0.19 nm These XRD data confirm the computed results for TM and TMC. The aggregates from the most concentrated sample in Fig. 4b were also investigated, which were prepared by filtering the solution prepared as in the UV experiment. The XRD curve showed the sample has an amorphous phase structure with one broad peak at 16°.

With the large free volume in crystal state, TM molecule is expected to be compressible, and TM should possess the piezochromical behavior. According to Tang's restriction of intramolecular rotations (RIR) mechanism[29] of AIE molecules, void volumes exist between the TM molecules in its crystal state to admit that they to adopt a state in which the phenyl rings are quite staggered placed, which reduces the intramolecular interaction. The restriction of phenyl rotations by the molecular interaction limits both the planarization and the π-conjugation. Emission of the crystal state is blue. While exerting external force to the crystal powder (physical grinding), the pressurization reacts against the intramolecular interaction, thus decreases the void volumes and densifies the molecular packing, causing the angles between phenyl rings planes decrease. The molecules become more planar. Therefore it increases the electron delocalizations and lowers the energy band gap of TM molecule, leading to a bathochromical shift in fluorescence emission to a green-yellow light (shown in Fig. 4c). A similar transformation has been observed in another of our former experiment. When amorphous TM treated with DCM steam, the fluorescence hypochromatically shifts from yellow-green to blue. The amorphous solid can be infiltrated with solvent molecules, enlarging the intermolecular space and activate the rotation of phenyl rings, ultimately reducing the molecular conjugation length and increasing the band gap. Thus the emission of steam treated samples turns back to a short wavelength of blue.

2.3. Electrical properties

The fluorescent mechanism discussed above is also supported by the electrochemical tests and DFT calculations. CV measurements and DFT calculations on TM and TMC are summarized in Table 1and Fig.5. The HOMO of TM and TMC come at –6.51 and –5.35 eV, respectively, and the LUMO energy levels that come at –1.94 and –3.55 eV with respect to ferrocene can be deducted from the onset potential of the oxidation and reduction, respectively. The band gaps of TM and TMC are 4.22 eV and 1.80 eV, respectively. In comparison, the DFT calculations gave 1.987 eV and 1.275 eV. Although, there is poor agreement between experiment and calculation, the trend is conserved. This implies that for TM and TMC, the band gap is narrowed by enlarging the delocalization in the less twisted molecule.

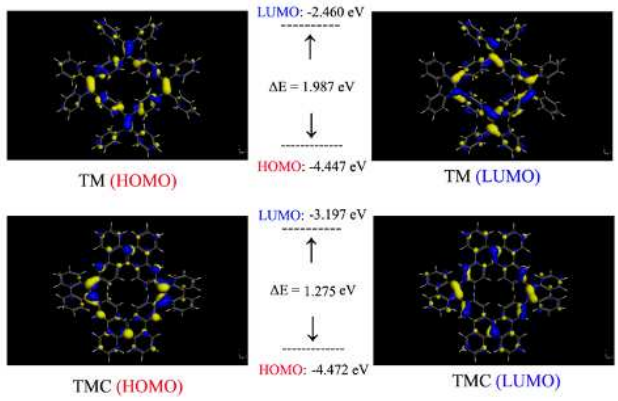

Fig. 5 Molecular orbital amplitude plots of the HOMO and LUMO energy levels of TM and TMC.

Table 1. Electrochemical Properties of the Macrocycles TM and TMC

Macrocycle	E onset ox (V)	E onset red (V)	HOMO (eV)		LUMO (eV)		E g (eV)	
			Exptl	Calc	Exptl	Calc	Exptl	Calc
TM	1.55	–2.67	–6.51	–4.447	–1.94	–2.460	4.22	1.987
TMC	0.60	–1.20	–5.35	–4.472	–3.55	–3.197	1.80	1.275

[a] Determined from the cyclic voltammetry in acetonitrile for the oxidation potentials, and in THF for the reduction potentials (0.1 M n-$Bu_4N^+PF_6^-$ as the supporting electrolyte) using Ag/Ag^+ (0.01 M) as a reference electrode at a scan rate of 100 mV/s.

[b] The HOMO and LUMO levels were determined using the following equations: HOMO/LUMO = - e (E_{onset} - 0.0468 V) - 4.8 eV, where 0.0468 V corresponds to FOC vs Ag/Ag^+.

To obtain a direct structure/property relationship for TM and TMC, we used the space-charge limited-current (SCLC) method suggested by Wu's group[30] to determine the charge carrier mobility. The device is a sandwich structure composed of ITO/PEDOT:PSS/(TM or TMC)/Au. The ITO acted as one electrode and the other was gold, cast by thermal evaporation to 200 nm. The TM or TMC film was made by drop casting from a DCM solution to a thickness of 2 μm. The charge carrier mobility is based on the following formula:

$$\mu = 8Jd^3 / 9\varepsilon_0\varepsilon_r V^2$$

Where J is the measured current density, μ the charge mobility, ε_0 the permittivity of free space, ε_r the dielectric constant of the material (a value of ε_r = 3 is assumed here), V the applied voltage, and d the thickness of the device. The measured mobilities for TMC and TM were 0.7022 and 0.0055 $cm^2 V^{-1} s^{-1}$ (shown in Fig. 6), respectively. The augmentation of mobility from TM to TMC (increased by ~ 10^2) is suggested by the significantly stronger π-π interaction in the less twisted molecule TMC than in TM.

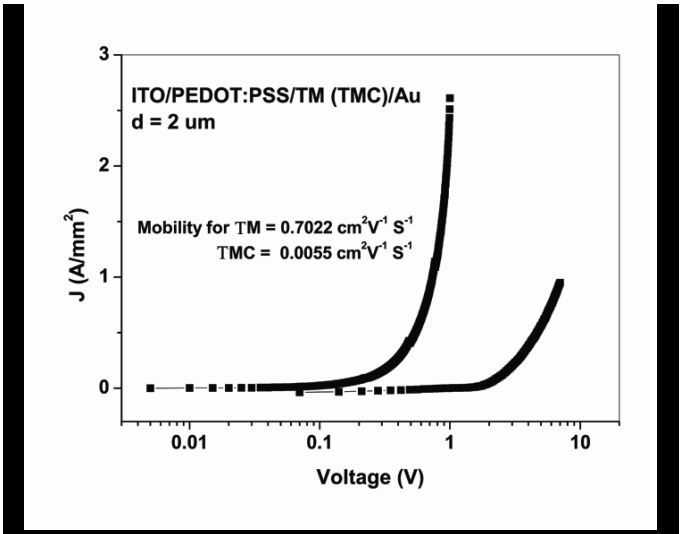

Fig. 6 Plot of the current density (J) versus applied voltage (V) measured across a 2.0 μm thick sample of TM and TMC at room temperature.

2.4. Thermal stabilities

The thermal stability of TM and TMC were evaluated by TGA under nitrogen at a heating rate of 10 °C min^{-1}. The compounds are thermally stable, losing 5% of their weight at 342 °C and 455 °C for TM and TMC, respectively (Fig. S6, ESI†). Both TM and TMC consist of only carbon and hydrogen atoms, and rich in carbon proportions. The strong carbon-carbon bonds and carbon-hydrogen bonds are relatively inert chemically, contributing to their high thermal stabilities. In addition, TMC molecule has a more planar structure, and it is observable that the peripheral phenyl rings form new carbon-carbon bonds by cyclodehydrogenation and are restricted and stabilized from free rotations, resulting in a relatively higher decomposition temperature of more than 100 °C than TM. The good thermal stabilities of TM and TMC are advantageous for their applications in optoelectronic devices. The results also suggest a viable way to increase thermal stability by cyclodehydrogenation.

3. Conclusion

We have synthesized a tetraphenylethene macrocycle (TM) from 1,1-bis(4-phenylcarbonyl)-2,2-diphenylethene by the McMurry coupling reaction in 45% yield. After chemical oxidation, a less twisted compound TMC was also obtained. These two derivatives clearly show the relationships between the conformations and the emission properties. TM has a twisted form and a short conjugated length. Its solid film luminescence is blue shifted compared with its solution emission. On the other hand, TMC has a less twisted conformation and hence is more conjugated, which induces the aggregation and a red shift in the emission. The different conformations also cause variations in the electrical properties. The CV characterization, charge mobility test and computer calculation prove the less twisted space-structured TMC has higher charge mobility than TM. The characterization results indicate that the macrocycles are qualified for potential materials in applications as field-effect transistors, light-emitting diodes etc. Similar approaches in molecular modification could also be efficient in adjusting molecular optical and electrical properties.

4. Experimental sections

Chemicals. Chemicals and reagents were purchased from Aldrich and Acros Chemical Co. unless otherwise stated and used without further purification. All of the solvents were used after purification according to conventional methods when required.

Measurements and characterizations. ^{1}H and ^{13}C NMR spectra were recorded with Varian Mercury Plus 400 spectrometers, and chemical shifts were reported in ppm units with tetramethylsilane as an internal standard. The UV-visible absorption spectra were obtained in chloroform on a Shimadzu UV-3150 spectrophotometer. The photoluminescence spectra were recorded on a Shimadzu RF-5301 PC fluorometer at room temperature. The samples were analyzed by Voyager DE-STR matrix assisted laser desorption-time-of-flight mass spectrometry (MALDI-TOF). Cyclic voltammetry (CV) measurements of the oligomer films coated on a glassy carbon electrode (0.08 cm^2) were performed in an electrolyte of 0.1 M tetrabutylammonium hexafluorophosphate ($TBAPF_6$) in acetonitrile using ferrocene (4.8 eV under vacuum) as the internal standard at a scan rate of 100 mV s^{-1} at room temperature under the protection of argon. A Pt wire was used as the counter electrode and an $Ag/AgNO_3$ electrode was used as the reference electrode. X-ray crystallographic data were collected on a P4 Bruker diffractometer equipped with a Bruker SMART 1K CCD area detector (employing the program SMART) and a rotating anode utilizing graphite-monochromated Mo KR radiation (λ) 0.710 73 Å). Data processing was carried out by use of the program SAINT, while the program SADABS was utilized for the scaling of diffraction data, the application of a decay correction and an empirical absorption correction based on redundant reflections. The structures were solved by using the direct-methods procedure in the Bruker SHELXL program library and refined by full-matrix least-squares methods on F2. All non-hydrogen atoms were refined using anisotropic thermal parameters, and hydrogen atoms were added as fixed contributors at calculated positions, with isotropic thermal parameters based on the carbon atom to which they are bonded.

Synthesis and characterization of 1,1-bis(4-phenylcarbonyl)-2,2-diphenylethene (1) and 1,2-bis(4-phenylcarbonyl)-1,2-diphenylethene (2). A stirred slurry of 2.66 g (0.02 mol) of aluminum chloride and 3.32 g of TPE (0.01 mol) in 15 mL of CS_2 was added dropwise with a solution of 1.41 g (0.01 mol) of benzoylchloride in 5 mL of CS_2 in room temperature. After that, water was cautiously added to the mixture on an ice bath. The reaction mixture was extracted by dichloromethane. The organic layer was washed with sodium hydroxide, dried with magnesium sulfate. The solvent was removed by rotary evaporation to yield a yellow green solid (3.1 g, 57%).

Two types of diketone of **1** and **2** in the crude product were separated by a silica column, giving a white solid of **1** and a yellow green crystal of **2** (petroleum ether : dichloromethane = 7 : 3; the R_f values are 0.60 for **1** and 0.67 for **2**).

(1). ^{1}H NMR ($CDCl_3$, 400 MHz): δ 7.72 - 7.77 (m, 4H), 7.52 - 7.62 (m, 6H), 7.42 - 7.48 (m, 4H), 7.08 - 7.18 (m, 10H), 7.02 - 7.08 (m, 4H). ^{13}C NMR ($CDCl_3$, 100 MHz): δ 127.5, 128.1, 128.4, 130.1, 131.5, 132.5, 135.7, 137.8, 139.1, 142.9, 144.4, 147.9, 196.5. m.p. 209 – 210 °C. Anal. Calcd for $C_{40}H_{28}O_2$ (540.65): C, 88.86; H, 5.22. Found: C, 88.80; H, 5.41. HRMS (MALDI-TOF): m/z 539.8 (M^+, 100%) , 562.8 ($[M+Na]^+$, 55%). Crystal data for **1**: crystals were grown from CH_2Cl_2; the structure was solved on a Bruker SMART CCD diffractometer using Mo K_α radiation. $C_{40}H_{28}O_2$ (*M*r = 540.62); monoclinic, space group *C*2/*c*, *D*c=1.233 g cm^{-3}, a =16.698(3) Å, b = 10.5516(19) Å, c = 16.706 (3) Å, α= 90°, β= 98.437(2)°, γ= 90°, V = 2911.6(9) $Å^3$, Z = 4, λ = 0.710 73 Å, μ = 0.075 mm^{-1}, T = 296(2) K, R = 0.0264 for 11 361 observed reflections [$I > 2\sigma I$] and R_w = 0.0939 for all 3138 unique reflections.

(2). ^{1}H NMR ($CDCl_3$, 400 MHz): δ 7.73 - 7.75 (m, 4H), 7.48 - 7.58 (m, 6H), 7.42 - 7.48 (m, 4H), 7.09 - 7.17 (m, 10H), 7.02 - 7.08 (m, 4H). ^{13}C NMR ($CDCl_3$, 100 MHz): δ 127.3, 128.1.5, 128.2, 129.7, 129.9, 131.2, 131.3, 132.3, 135.6, 137.8, 141.6, 142.6, 147.8, 196.2. m.p. 207-208 °C. Anal. Calcd for $C_{40}H_{28}O_2$ (540.65): C, 88.86; H, 5.22. Found: C, 87.71; H, 5.30. HRMS (MALDI-TOF): m/z 539.8 (M^+, 100%), 562.8 ($[M+Na]^+$, 47%). Crystal data for **2**: crystals were grown from CH_2Cl_2; the structure was solved on a Bruker SMART CCD diffractometer using Mo K_α radiation. $C_{40}H_{28}O_2$ (*M*r = 540.62); monoclinic, space group *C*2/*c*, *D*c=1.219 g cm^{-3}, a = 17.821(7) Å, b = 12.088(5) Å, c = 28.577(12) Å, α= 90°, β= 106.795(7)°, γ= 90°, V = 5894(4) $Å^3$, Z = 8, λ = 0.71073 Å, μ = 0.074 mm^{-1}, T = 296(2) K, R = 0.0461 for 15904 observed reflections [$I > 2\sigma I$] and R_w = 0.0684 for all 3013 unique reflections.

Synthesis of TM(3). A slurry of zinc (3.0 g) and tetrahydrofuran (30 mL) was stirred under a nitrogen atmosphere on an ice bath, and 5 mL of titanium tetrachloride was slowly dropped in. When finished, the ice bath was withdrawn. The mixture was heated by oil bath and refluxed for 30 min. Then, a solution of **1** (0.30g, 5.5 mmol) in tetrahydrofuran (30 mL) was added to the mixture. The reaction mixture was refluxed overnight. When cooled, the reaction was stopped by adding 10% potassium carbonate aqueous. The organic layer was extracted by dichloromethane and was dried by magnesium sulfate for 30 min. Dried organic layer was concentrated by rotary evaporation and was poured to a mixture of petroleum ether and ethyl acetate (9:1) to precipitate a single product of **3**. A white solid (0.13 g, 45%) was obtained by further filtration. ^{1}H NMR (CD_2Cl_2, 400 MHz): δ 7.07 - 7.06 (m, 24H), 6.96 - 6.71 (m, 16H),

6.70-6.68 (s, 16H). HRMS (MALDI-TOF): 1016.51. The solubility of TM in common d-solvents (like d-chloroform, d2-dichloromethane and other d-solvents) is low and cannot get the ^{13}C NMR.

Synthesis of TMC(4). 100 mg of pure TM was dissolved in 100 mL DCM. The solution was deoxygenized by purging N_2. Ferric trichloride (2 g) was solved in 20 mL CH_3NO_2 and added to the solution with a continued purge of nitrogen. After stirring for 30 min at room temperature, 40 mL of methanol was added to quench the reaction. The precipitated product was filtered and washed with EA, ethanol and methanol to afford a red solid (0.85mg, yield 85%). ^1H NMR (CD_2Cl_2, 400 MHz): δ 7.77 -7.10 (m, 33H), 8.22 -10.24 (m, 11H). HRMS (MALDI-TOF): 1004.20. The solubility of TMC in common d-solvents (like d-chloroform, d2-dichloromethane and other d-solvents) is low and cannot get the ^{13}C NMR.

Acknowledgements

This work was financially supported by the National Natural Science Foundation of China (21274027 and 20974022). Wang Han thanks the FDUROP (Fudan's Undergraduate Research Opportunities Program) for support.

References and notes

1. Novoselov, K.S.; Geim, A.K.; Morozov, S.V.; Jiang, D.; Zhang, Y.; Dubonos, S.V. *Science* **2004**,306, 666-669.
2. Geim, A. K. *Science* **2009**, 324, 1530-1534.
3. Berger, C.; Song, Z. M.; Li, X. B.; Wu, X. S.; Brown, N.; Naud, C.; Mayou, D.; Li, T. B.; Hass, J.; Marchenkov, A. N.; Conrad, E. H.; First P. N.; de Heer, W. A. *Science* **2006**, 312, 1191-1196.
4. Zhang, Y. B.; Tan, Y. W.; Stormer H. L.; Kim, P. *Nature* **2005**, 438, 201-204.
5. Yang, L.; Park, C. H.; Son, Y. W.; Cohen M. L.; Louie, S. G. *Phys. Rev. Lett.* **2007**, 99, 186801.
6. Barone, V.; Hod, O.; Scuseria, G. E. Nano. Lett. **2006**, 6, 2748-2754.
7. Avouris, P.; Chen Z. H.; Perebeinos, V. *Nature Nanotechnology* **2007**, 2, 605-615.
8. Schwierz, F. *Nature Nanotechnology* **2010**, 5, 487-496.
9. Kim, K. S.; Zhao, Y.; Jang, H.; Lee, S. Y.; Kim, J. M.; Kim, K. S.; Ahn, J. H.; Kim, P.; Choi, J. Y.; Hong, B. H. *Nature* **2009**, 457, 706-710.
10. Bonaccorso, F.; Sun, Z.; Hasan T.; Ferrari, A. C. *Nature Photonics* **2010**, 4, 611-622.
11. Schniepp, H. C.; Li, J. L.; McAllister, M. J.; Sai, H.; Herrera-Alonso, M.; Adamson, D. H.; Prud'Homme, ; Car, R.; Saville, D. A. Aksay, I. A. *J. Phys. Chem. B* **2006,** 110, 8535-8539.
12. Berger, C.; Song, Z. M.; Li, T. B.; Li, X. B.; Ogbazghi, A. Y.; Feng, R.; Dai, Z. T.; Marchenkov, A. N.; Conrad, E. H.; First, P. N.; de Heer, W. A. *J. Phys. Chem.* B **2004**, 108, 19912-19916.
13. Reina, A.; Jia, X. T.; Ho, J.; Nezich, D.; Son, H. B.; Bulovic, V.; Dresselhaus, M. S.; Kong, J. *Nano. Lett.* **2009**, 9, 30-35.
14. Li, X. S.; Cai, W. W.; An, J. H.; Kim, S.; Nah, J.; Yang, D. X.; Piner, R;. Velamakanni, A.; Jung, I.; Tutuc, E.; Banerjee, S. K.; Colombo, L.; Ruoff, R. S. *Science* **2009**, 324, 1312-1314.
15. Wagner, P.; Ewels, C. P.; Ivanovskaya, V. V.; Briddon, P. R.; Pateau, A. Humbert, B. *Phys. Rev. B* **2011**, 84, 134110.
16. Wu, J. S.; Pisula, W.; Müllen, K. Chem. Rev. **2007**, 107, 718-747.
17. Feng, X. L.; Wu, J. S.; Enkelmann, V.; Müllen, K. *Org. Lett.* **2006**, 8, 1145-1148.
18. Wu, J. S.; Tomović, Ž.; Enkelmann, V.; Müllen, K. *J. Org. Chem.* **2004,** 69, 5179-5186.
19. Dötz, F.; Brand, J. D.; Ito, S.; Gherghel, L.; Müllen, K. *J. Am. Chem. Soc.* **2000**, 122, 7707-7717.
20. Müller, M.; Kübel, C.; Müllen, K. *Chem-Eur. J.* **1998**, 4, 2099-2109.
21. Simpson, C. D.; Brand, J. D.; Berresheim, A. J.; Przybilla, L.; Räder, H. J. Müllen, K. *Chem-Eur. J.* **2002**, 8, 1424-1429.
22. Cai, J. M.; Ruffieux, P.; Jaafar, R.; Bieri, M.; Braun, T.; Blankenburg, S.; Muoth, M.; Seitsonen, A. P.; Saleh, M.; Feng, X. L.; Müllen, K. ; Fasel, R. *Nature* **2010**, 466, 470-473.
23. Esser, B.; Rominger, F.; Gleiter, R; *J. Am. Chem. Soc.* **2008**, 130, 6716-6717.
24. Hitosugi, S.; Yamasaki, T; Isobe, H.; *J. Am. Chem. Soc.* **2012**, 134, 12442-12445.
25. Przybilla, L.; Brand, J. D.; Yoshimura, K.; Räder, H. J.; Müllen, K. *Anal. Chem.* **2000**, 72, 4591-4597.
26. Dong, Y. Q.; Lam, J.; Qin, A. J.; Liu, J. Z.; Li, Z.; Tang, B. Z. *Appl. Phys. Lett.* **2007**, 91, 011111.
27. Wang, W. Z.; Lin, T. T.; Wang, M.; Liu, T. X.; Ren, L. L.; Chen, D.; Huang, S. J. Phys. Chem. B **2010**, 114, 5983-5988.
28. Hong, Y.; Lam, J. W. Y.; Tang, B. Z. Chem. Soc. Rev. **2011**, 40, 5361-5388.
29. Hong, Y.; Lam, J. W. Y.; Tang, B. Z. *Chem. Commun.* **2009**, 29, 4332 - 4353.
30. Zhang, X. J.; Jiang, X. X.; Zhang, K.; Mao, L.; Luo, J.; Chi, C. Y.; Chan, H.; Wu, J. S. *J. Org. Chem.* **2010**, 75, 8069-77.

Supplementary Material

Supplementary information (NMR spectra and single crystal structures of monomer **1** and **2**; MALDI-TOF for McMurry coupling of monomer **2**; MALDI-TOF and ^1H NMR spectra of TM and TMC; PL spectra of TM in varied proportion of DCM/PE solutions; CV experiments of TM and TMC; TGA of TM and TMC; DFT calculations of TPE, TM, TMC and $C_{80}H_{40}$.) can be found at

Supporting Information

Synthesis and properties of a graphene-like macrocycle based on tetraphenylethene

Han Wang,[a] Tingting Lin,[b] Ji Ma,[a] Weizhi Wang*[a]

[a]State Key Laboratory of Molecular Engineering of Polymers, Department of Macromolecular Science, Fudan University, Shanghai 200433, China

[b]Institute of Materials Research and Engineering, A*STAR (Agency for Science, Technology and Research), 3 Research Link, Singapore 117602.

Table S1. The NMR data and crystal structures for monomer **1** and **2**.

Monomer 1	Monomer 2
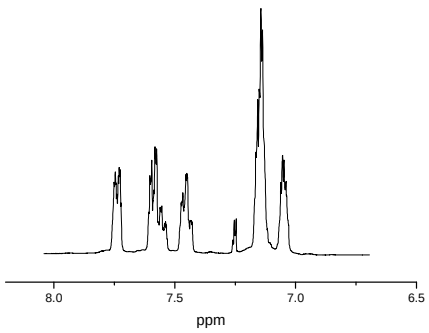	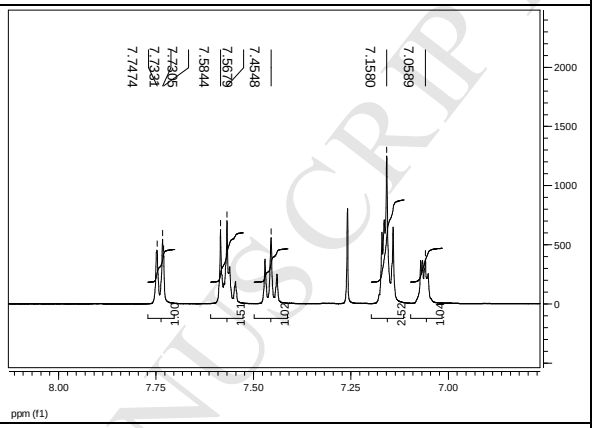
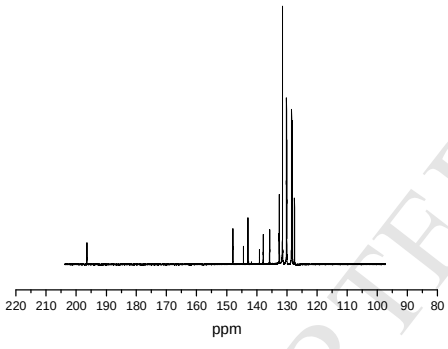	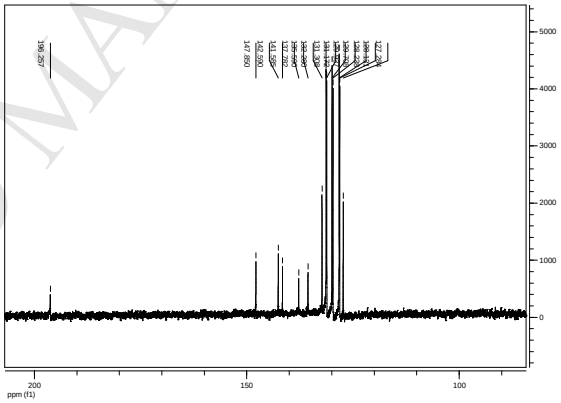
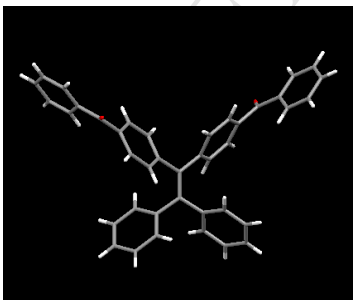	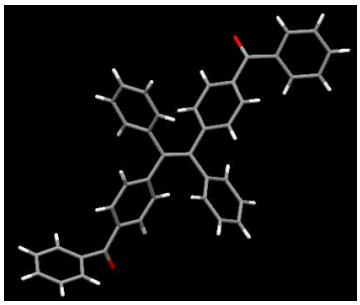

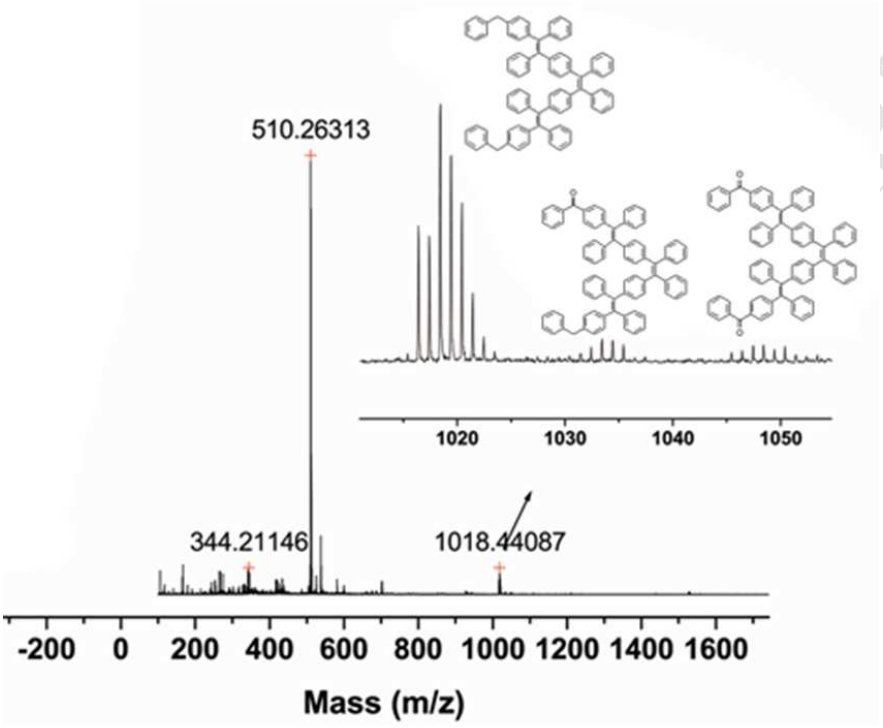

Fig. S1 MALDI-TOF of McMurry coupling for monomer **2**. Isomers may exist in the coupling products.

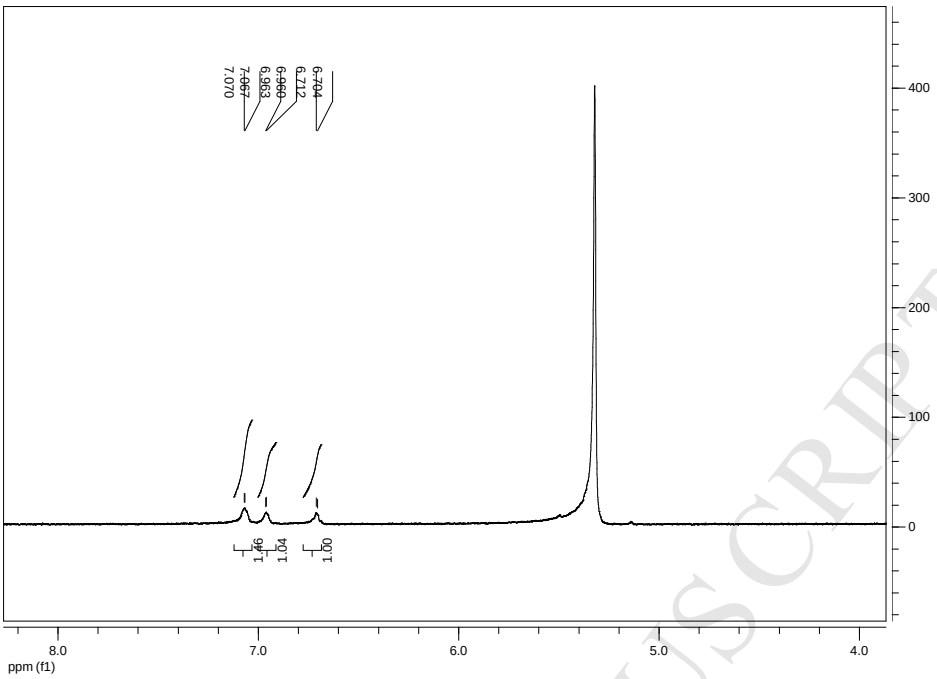

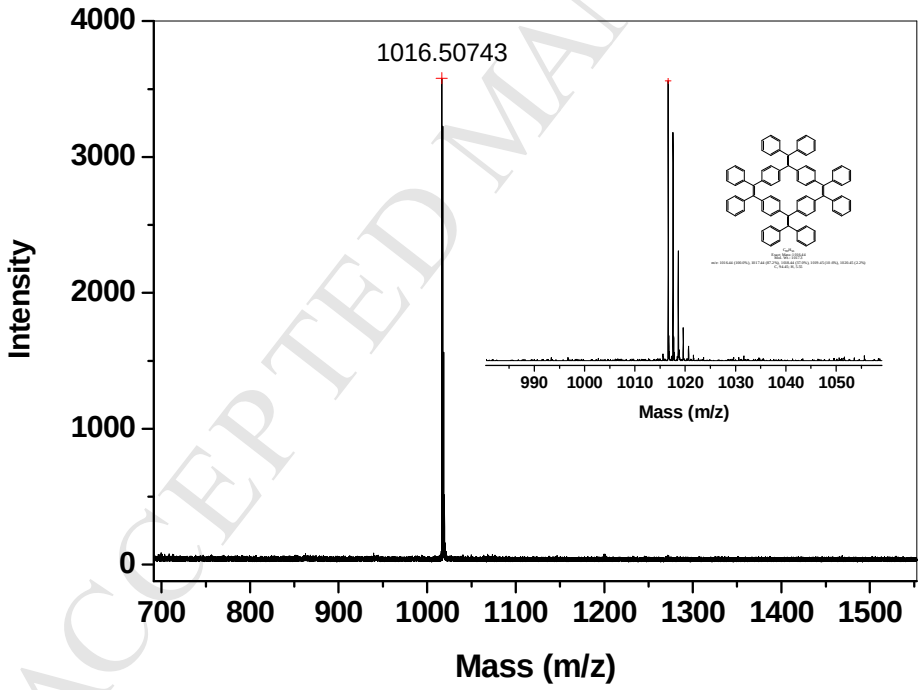

Fig. S2 The ^{1}H-NMR and MALDI-TOF of TM.

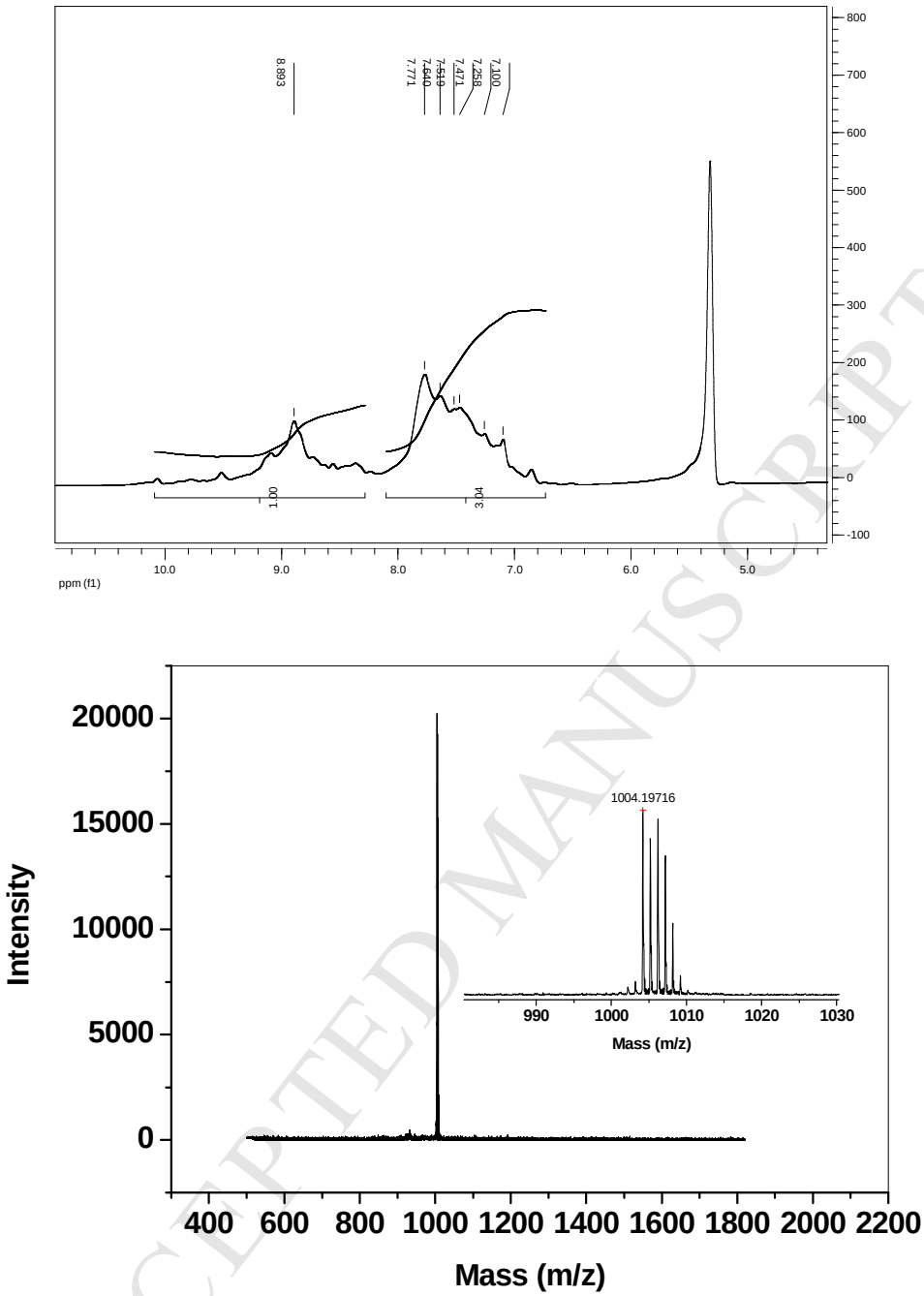

Fig. S3 The ^{1}H-NMR and MALDI-TOF of TMC.

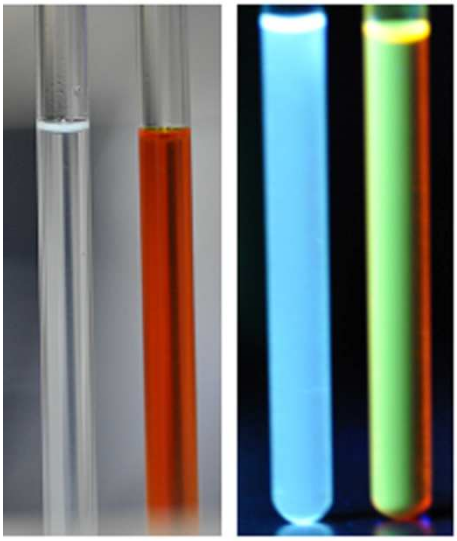

Fig. S4 The pictures of TM (colorless) and TMC (red) solutions under natural light (left) and 365 nm UV irradiation (right).

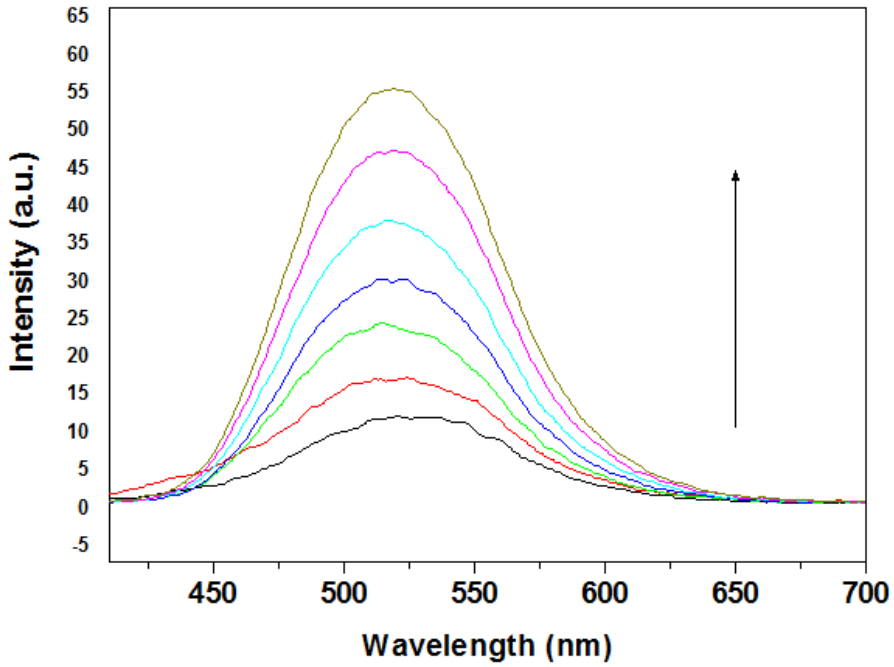

Fig. S5 (a) PL spectra of TM in DCM and DCM/PE mixtures with different PE fractions. (b) Change in the relative PL intensity (I/I_0) with the composition of the DCM/PE mixture. I_0 = PL intensity in pure DCM solution. Concentration: 3.0 μM ; excitation wavelength: 360 nm.

Table S2. The CV experiments of TM and TMC.

TMC	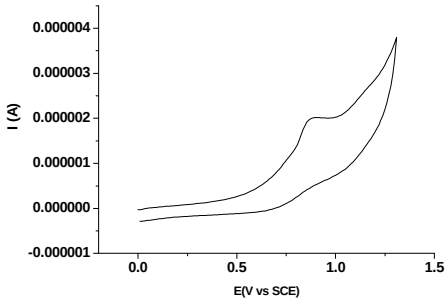	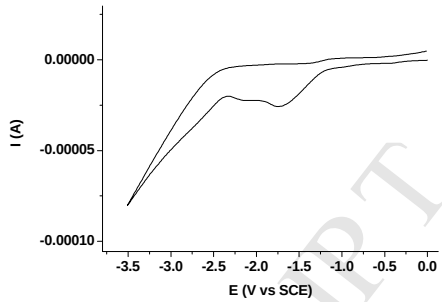
TM	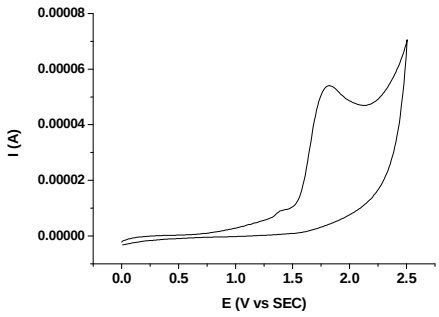	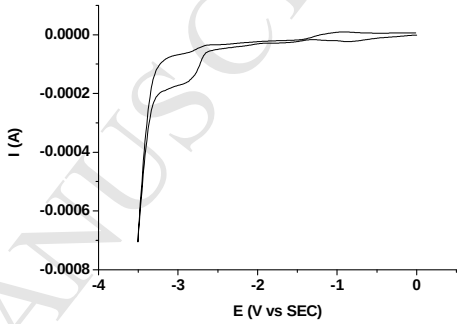

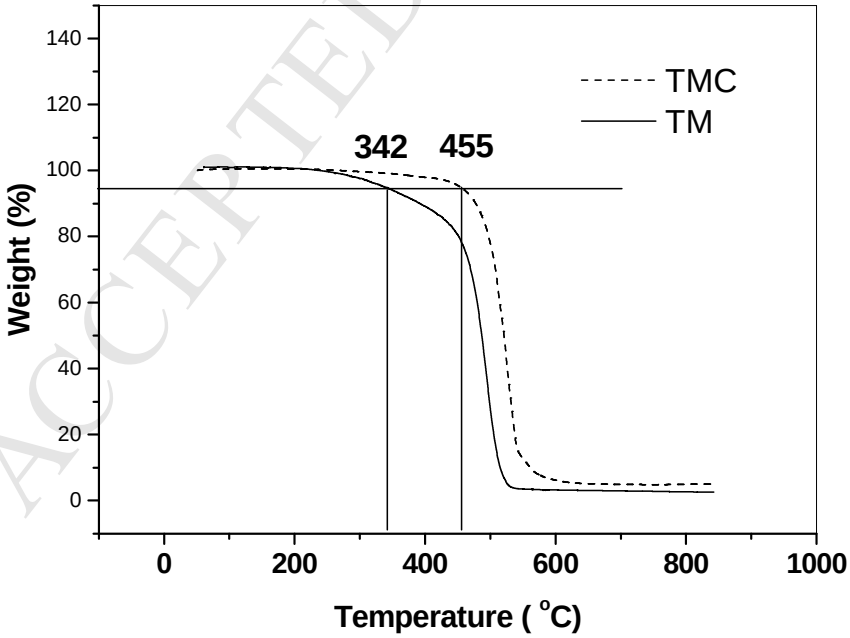

Fig. S6 The thermal weight loss curves of TM and TMC.

Density functional theory (DFT) computations: The molecular models (as listed in Table S3) were built by using Materials Studio v.5.0 (Accelrys Software Inc.). The structures were optimized at the level of theory GGA-PW91-dspp/dnp (with a orbital cutoff of 3.7 Å) by using the DFT module DMol^3 (refs: B. Delley, *J. Chem. Phys.* 1990, **92**, 508. B. Delley, *J. Chem. Phys*. 2000, **113**, 7756.) in Materials Studio. The HOMO, LUMO and other properties were obtained at the DFT optimized geometries. The geometric properties (torsion angles, bond lengths), HOMO and LUMO are illustrated in Fig. S7 to S10.

Table S3. A summary of DFT calculations.

Molecule	Mass	HOMO (eV)	LUMO (eV)	Gap (eV)	vdW surface		(accessible) Solvent surface @ 1.4	
					Occupied Volume (Å)^3	Surface area (Å)^2	Occupied Volume (Å)^3	Surface area (Å)^2
$C_{80}H_{56}$ (TM)	1017.33	-4.447	-2.460	1.987	969.57	978.32	2690.12	1279.42
$C_{80}H_{44}$ (TMC)	1005.23	-4.472	-3.197	1.275	893.12	842.86	2385.44	1195.26
$C_{80}H_{40}$	1001.20	-4.672	-2.882	1.790	873.73	805.63	2305.58	1183.97
$C_{26}H_{20}$ (TPE)	332.446	-4.879	-2.216	2.663	326.41	368.70	1006.64	592.81
$C_{40}H_{28}O_2$ (monomer 1)	540.662							
$C_{40}H_{28}O_2$ (monomer 2)	540.662							

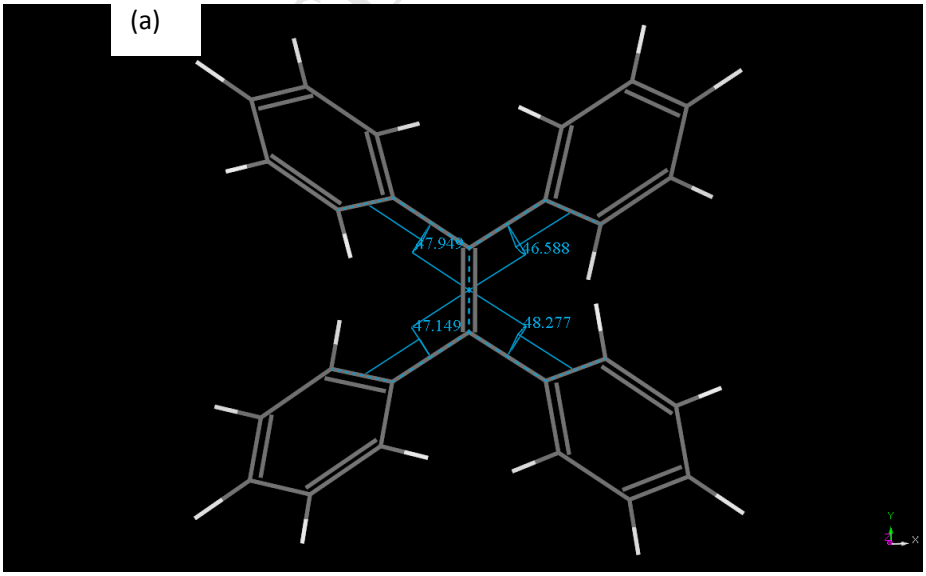

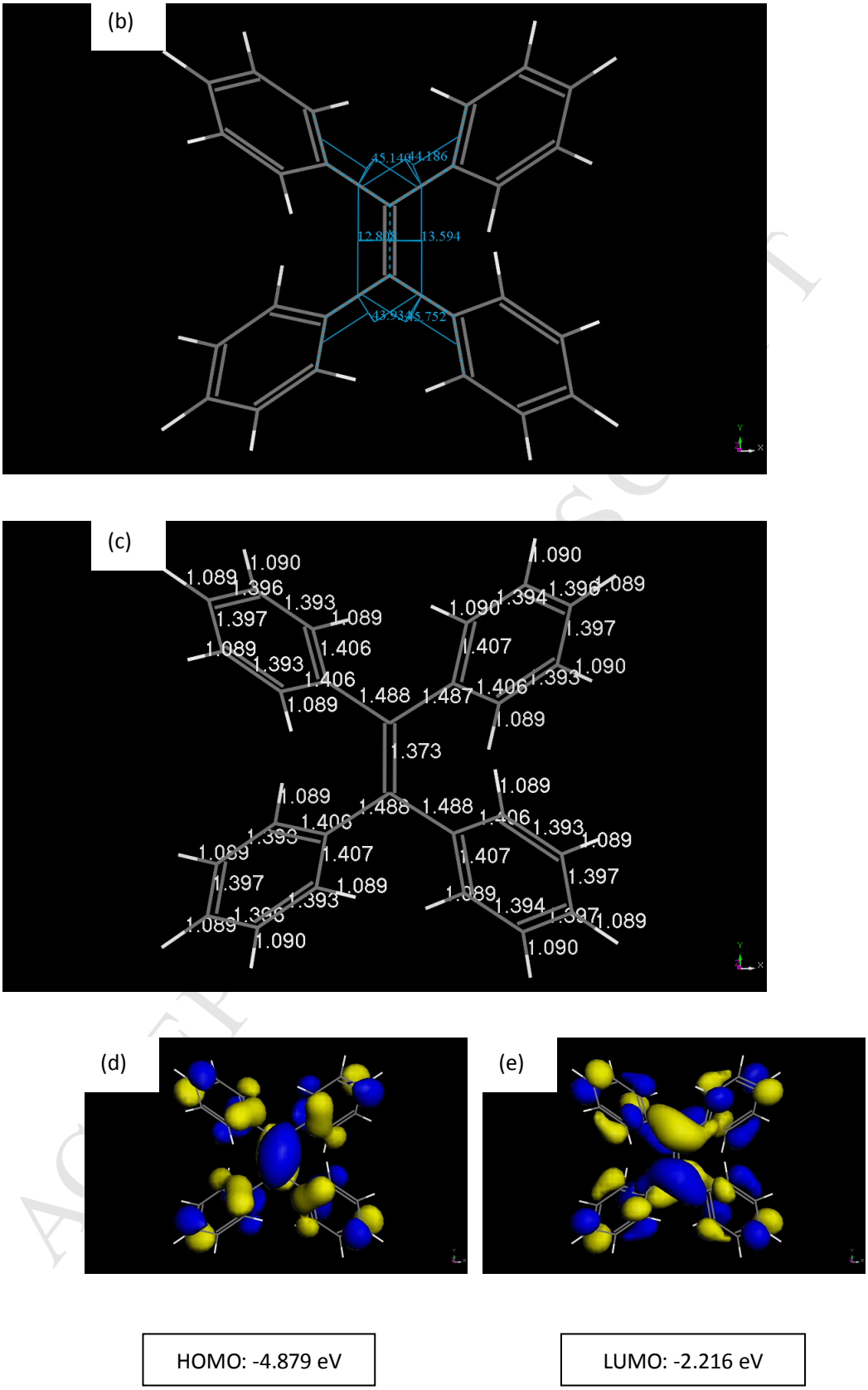

Fig. S7 The DFT optimized structure of TPE ($C_{26}H_{20}$): (a) and (b) torsion angles (in degree); (c) bond lengths (in Å); (d) HOMO (e) LUMO. (plotted with isovalue 0.03).

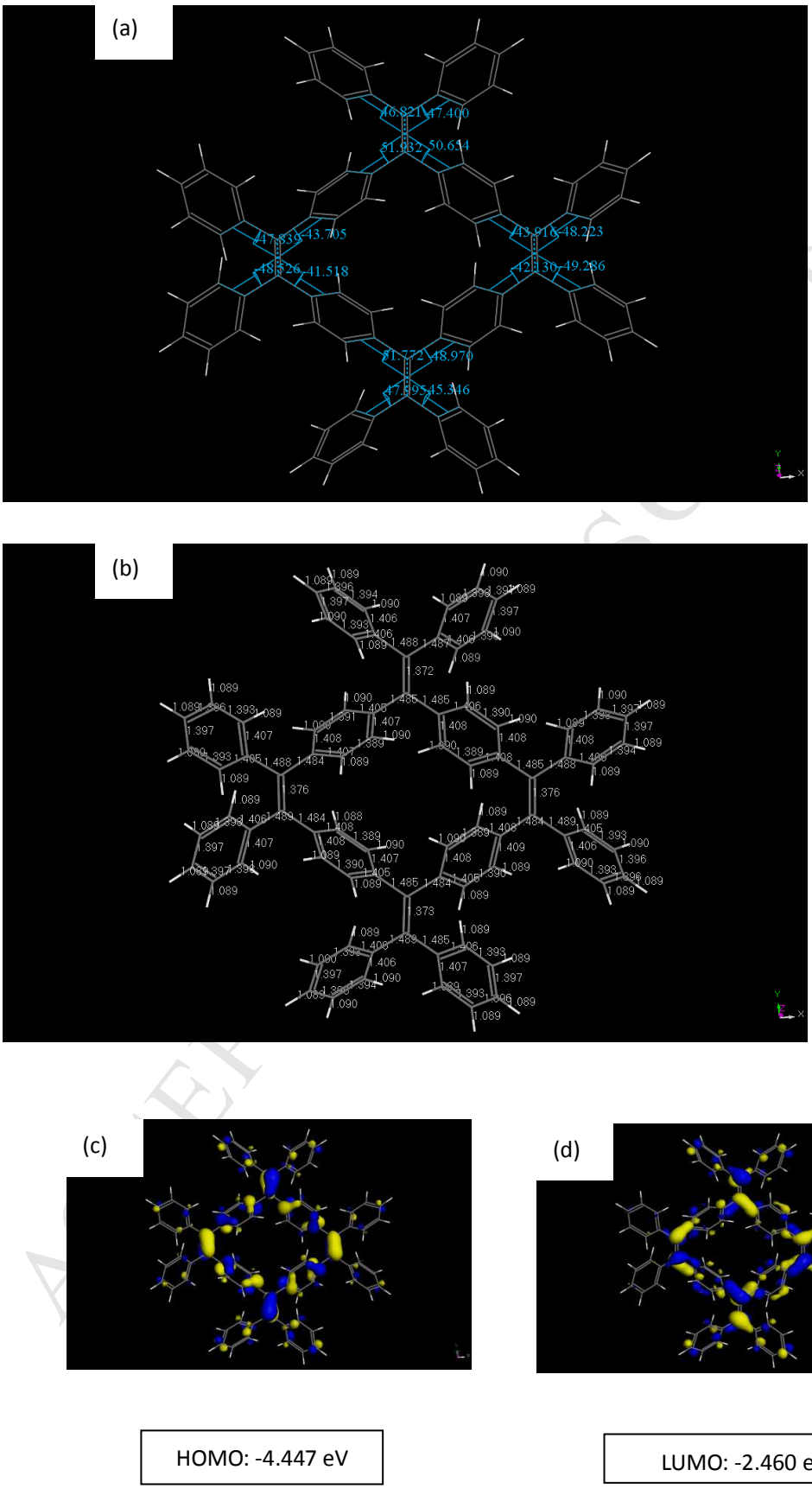

Fig. S8 The DFT optimized structure of TM ($C_{80}H_{56}$): (a) torsion angles (in degree); (b) bond lengths (in Å); (c) HOMO (d) LUMO. (Plotted with isovalue 0.03).

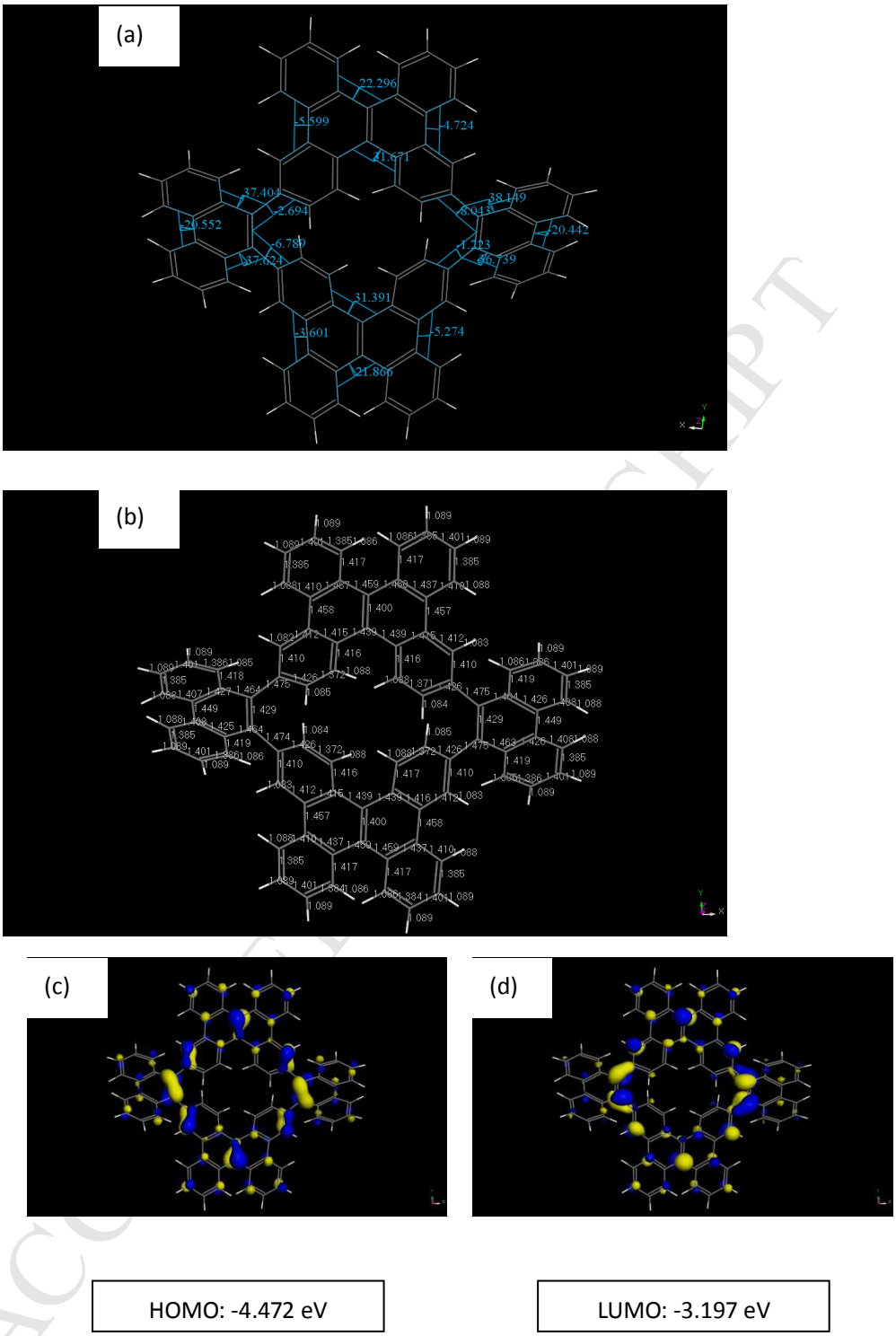

Fig. S9 The DFT optimized structure of TMC ($C_{80}H_{44}$): (a) torsion angles (in degree); (b) bond lengths (in Å); (c) HOMO (d) LUMO. (Plotted with isovalue 0.03). The torsion angles reduce significantly compared to TPE or TM, however the fused rings twist.

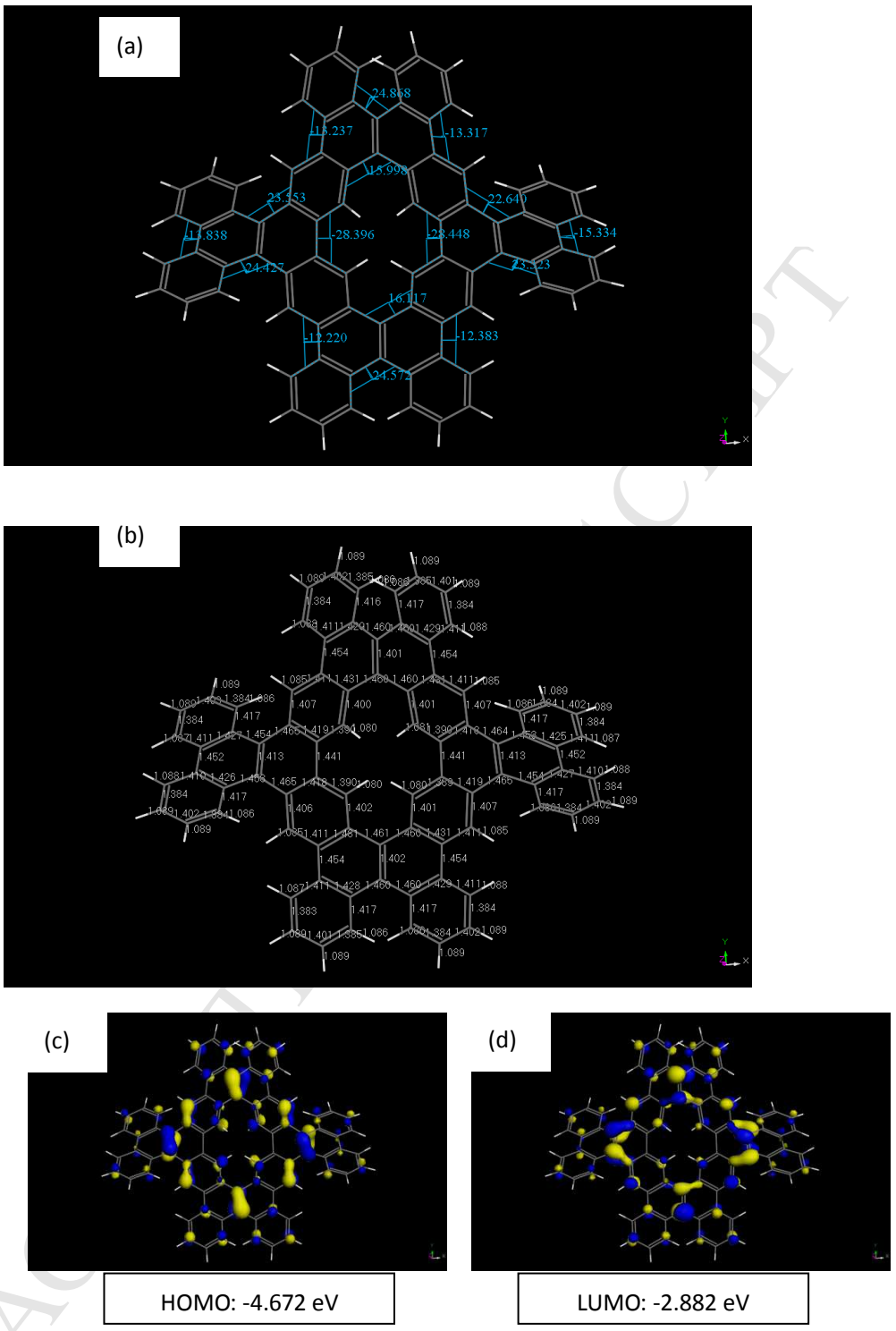

Fig. S10 The DFT optimized structure of $C_{80}H_{40}$: (a) torsion angles (in degree); (b) bond lengths (in Å); (c) HOMO (d) LUMO. (Plotted with isovalue 0.03).